PAPER

Enhanced Cr(VI) removal by Co and PPy co-modified Ca–Al-layered double hydroxides due to adsorption and reduction mechanisms†

Wenyan He, [ID] *[ab] Kaijie Ye,[a] Mi Zhang,[a] Sheng Bai,[a] Siyan Xu[a] and Kuo Fang[c]

Co and polypyrrole co-modified hierarchical CaAl-LDH microspheres (CCALP) were synthesized *via* hydrothermal and *in situ* polymerization methods. The synergistic effect of PPy and Co endowed CCALP with higher surface area and more reduction sites than CaAl-LDHs modified by Co or PPy alone, maintaining good recyclability for Cr(VI) removal efficiency over four cycles without any treatment. Compared to Co, PPy doping was the dominant reason for Cr(VI) reduction on CCALP. Under optimized conditions, the theoretical maximum adsorption capacity reached 845.25 mg g^{-1}, and the removal efficiency of Cr(VI) achieved 98.83%. The Langmuir model fitted well with the Cr(VI) adsorption on CCALP, supporting the monolayer adsorption hypothesis. The adsorption process followed the Avrami fractional kinetics (AFO) model, suggesting complex and multiple kinetic stages. Thermodynamic experiments confirmed that the adsorption was a spontaneous exothermic process. The density functional theory (DFT) and electrostatic potential (ESP) calculations confirmed that the oxygen-containing parts of $Cr_2O_7^{2-}$ and $HCrO_4^{-}$ were the affinity sites, and the co-doping of Co and PPy significantly improved the Cr(VI) adsorption energy on CCALP. Therefore, the Cr(VI) removal mechanism on CCALP was proposed with electrostatic interaction, ion exchange, complexation and reduction.

1 Introduction

Excess release of heavy metals into water bodies has aroused widespread concern due to their high toxicity, long half-times, bioaccumulation in organisms, and biomagnification in the food chain, posing an enormous threat to human beings and ecosystems.[1] Chromium, a foremost typical heavy metal pollutant, exists mainly in the forms of Cr(III) and Cr(VI). The latter is in the forms of CrO_4^{2-}, $HCrO_4^{-}$ and $Cr_2O_7^{2-}$, 100 times more toxic to biological systems[2] because of its strong solubility and easy migration, carcinogenicity and teratogenicity.[3,4] Tseng *et al.*[5] found that Cr(VI) contamination leads to a 60-fold increase in the prevalence of gastric cancer, resulting in substantial loss of life expectancy and increased medical expenditure.

Accordingly, developing eco-friendly and cost-effective techniques for Cr(VI) removal from water is imperative to address the intertwined challenges of water security, environmental degradation, and energy consumption.[6] Precipitation,[7] membrane

separation,[8] ion exchange,[9] biological treatment,[10] flocculation,[11] and electrodialysis[12] have been widely investigated for Cr(VI) removal. However, high operation and maintenance costs, stability and regeneration difficulties limit their practical applications. Compared to the other methods, adsorption is one of the most promising techniques due to its low cost and simplicity in preparation, operation, and regeneration processes. Numerous adsorbents, including carbon,[13] covalent-organic framework,[4] metal–organic frameworks,[14] MXene,[15] chitosan biopolymer,[16] and clays[17,18] have been investigated for Cr(VI) removal. Besides, layered double hydroxides (LDHs) also have been widely studied. The formula of LDHs is $[M_{1-x}^{II}M_x^{III}(OH)_2]^{x+}(Anion^{n-})_{x/n} \cdot mH_2O)$, where the tunable M^{II+} (Mg^{2+}, Fe^{2+}, Ni^{2+}, Cu^{2+}, Co^{2+}, Mn^{2+}, Zn^{2+} or Cd^{2+}, *etc.*) and M^{III+} (Al^{3+}, Cr^{3+}, Ga^{3+} or Fe^{3+}, *etc.*) ratios construct different layered backbones, and counter-anions (CO_3^{2-}, SO_4^{2-}, Cl^-, NO_3^-, organic anions) in the interlayer space stabilize the structure and balance the charge.[19–21] Therefore, the excellent intercalation, anion exchangeability, and two-dimensional layered structure with adjustable specific surface areas make LDHs remarkable environmentally friendly adsorbents.[22–25]

CaAl-LDH, one of the most concerned LDHs, has been extensively studied for various pollutant removal.[26–28] Qiu *et al.*[25] found that CaAl-LDHs significantly improve the removal rate of phosphate, regardless of whether the calcium and aluminum sources for preparing LDHs come from chemical reagents or solid waste. Functionalized LDHs have been constructed by

[a]College of Geology and Environment, Xi'an University of Science and Technology, Xi'an 710054, China. E-mail: wenyanhe001@xust.edu.cn; Tel: (+8629) 8558-3188

[b]Shaanxi Provincial Key Laboratory of Geological Support for Coal Green Exploitation, Xi'an University of Science and Technology, Xi'an 710054, China

[c]College of Chemical Engineering, Beijing University of Chemical Technology, Beijing, 100029, China

incorporating various components, such as anion or transition metal ions, which significantly impact the morphology and properties of the composites, further upgrading the adsorption capacity. For example, thiosulfate ions were applied to improve the interlayer distance of the CaAl-LDHs, achieving high adsorption performance towards the malachite green from an aqueous solution.[27] Besides, as the component of the LDHs structure, metal cations such as Co^{2+}, Fe^{2+}, La^{3+}, and Zn^{2+} play a vital role in the adsorption performance.[3] Compared to the other cationic-modified MgAl-LDH, CoMgAl-LDH exhibited the highest adsorption capacity for Cr(VI) because its surface area steadily increased with increasing the Co content.[19] Moreover, Co ions could act as active centers, altering the surface charge of LDHs, thus providing more surface active sites for Cr(VI) adsorption through electrostatic attraction and other interactions. Furthermore, Co(II) has a certain reducibility, which can reduce part of Cr(VI) to Cr(III), thereby increasing the removal capacity of Cr(VI). However, the effect of Co on CaAl-LDH for Cr(VI) adsorption performance has not been investigated. Moreover, relying solely on electrostatic adsorption, ion exchange, and hydrogen bonds is insufficient to reduce the Cr(VI) toxicity.

Bearing the merits of low cost, high adsorption capacity, biocompatibility, nontoxicity, and high environmental stability,[2] polypyrrole (PPy) is rich in positively charged nitrogen atoms, enabling strong charge interactions with anion binding. Furthermore, PPy can effectively reduce harmful Cr(VI) to low-toxic Cr(III).[29] PPy-modified synthetic composites, such as magnetic corncob biochar/polypyrrole composites,[30] polypyrrole coated molybdenum disulfide composites,[31] graphene/SiO_2@polypyrrole nanocomposites,[32] polypyrrole decorated reduced graphene oxide–Fe_3O_4 magnetic composites,[33] have demonstrated tremendous application potential for Cr(VI) removal. Yang et al.[34] reported that the PPy-modified CaAl-LDH exhibited higher Cr(VI) adsorption capacity than that of the CaAl-LDH alone. However, a longer time was needed (180 minutes), and the maximum adsorption capacity was only about 66.14 mg g^{-1}. Besides, the tendency of PPy chains to reunite can negatively impact their adsorption efficiency. Whether these problems can be effectively solved through the doping of Co based on PPy-modified CaAl-LDH remains to be studied. Furthermore, elucidating the synergistic mechanisms underlying Cr(VI) adsorption is also momentous.

Herein, Co and PPy co-modified CaAl-LDH composites (CCALP) were synthesized via hydrothermal and in situ polymerization methods, demonstrating outstanding Cr(VI) removal efficiency. Initially, the experimental conditions were optimized, followed by an investigation into the adsorption isotherms, thermodynamics, and kinetics of the Cr(VI) adsorption processes. By comparing the physical and chemical properties of the materials before and after adsorption, the synergistic effect of PPy and Co on CCALP for Cr(VI) removal was revealed. Besides, DFT and ESP analyses were conducted to investigate the adsorption energy (E_{ads}) and active sites of the prepared adsorbents for Cr(VI) removal. This study provides new insights into the adsorption characteristics of Co and PPy on the structural and dynamical behavior of CaAl-LDHs, highlighting their potential for practical application.

2 Methods and materials

2.1 Materials

Potassium dichromate, sodium nitrate, and sodium hydroxide were purchased from Tianjin Kermel Chemreagent Co. Calcium nitrate tetrahydrate ($Ca(NO_3)_2 \cdot 4H_2O$) was purchased from Tianjin Bodi Chemical Co. Aluminum nitrate nonahydrate ($Al(NO_3)_3 \cdot 9H_2O$) and cobalt nitrate hexahydrate ($Co(NO_3)_2 \cdot 6H_2O$) were obtained from Tianjin Damao Chemical Reagent Factory. Pyrrole monomer was purchased from Shanghai Macklin Biochemical Co., Ltd. Phosphoric acid was obtained from Xilong Science Co., Ltd. All chemicals are analytic purity and used without further treatment.

2.2 Preparation of CCAL and CCALP

Preparation method of CCAL. The CoCaAl-layered double hydroxides with different Co : Ca : Al molar ratios were prepared via the hydrothermal method. For the Co : Ca : Al = 1 : 2 : 1, 4.80 g $Co(NO_3)_2 \cdot 6H_2O$, 7.56 g $Ca(NO_3)_2 \cdot 4H_2O$, and 6.18 g $Al(NO_3)_3 \cdot 9H_2O$ were dissolved in 100 mL 0.5 mol per L $NaNO_3$ solution, and the pH was adjusted and maintained at 12 ± 0.5. Then transferred to a polytetrafluoroethylene reaction kettle and put in an oven at 80 °C for 24 h. After cooling to room temperature, it was centrifuged at 6000 rpm for 5 min and then dried in a vacuum oven at 60 °C for 24 h. Before the adsorption experiment, it was ground and passed through a 100-mesh sieve, and the obtained powder was named CCAL.

Preparation method of CCALP. CCALP was prepared with different CCAL and PPy mass ratios via the in situ polymerization method. For CCAL : PPy = 1 : 0.07, 0.09 g of PPy monomer and 1.27 g of CCAL were added to 100 mL of deionized water and then placed in a thermostatic oscillator (30 ± 2 °C, 150 rpm, 30 min). Subsequently, 50 mL 140.6 g L^{-1} $FeCl_3$ solution, used as the oxidant, was added dropwise to the above solution and oscillated at 150 rpm and 30 °C for 24 hours, followed by centrifugation (6000 rpm, 5 min) and washing with deionized water several times. The obtained CCALP was subsequently dried in a vacuum oven at 60 °C for 24 h and passed through a 100-mesh sieve.

Besides, the CaAl-layered double hydroxides (CAL) and PPy-modified CaAl-layered double hydroxides (CALP) were prepared according to the above methods.

2.3 Structural characterization

SEM images and corresponding EDX-mappings were recorded by a Field emission scanning electron microscope (JSM-7610F, Japan) to investigate the morphological characteristics and elemental composition. X-ray photoelectron spectroscopy (XPS, Thermo Fisher) revealed the adsorbent surface elemental chemical environment before and after adsorption. N_2 adsorption–desorption isotherms were measured by a Mac ASAP 2020 instrument. The AFT-FTIR spectra were obtained on a Tensor 27 spectrophotometer (Bruker) to identify the functional groups

present on the surface of the composites. The crystal structure of the composites was investigated by a Bruker D8 powder X-ray diffractometer. The zeta potential of the adsorbents was performed on Zeta sizer Nano-ZS90 (Malvern Instruments, UK).

2.4 Batch adsorption experiments

The static adsorption experiments of Cr(VI) in aqueous were performed with CCALP adsorbent. The effects of the preparation parameters, such as the Co : Ca : Al molar ratio (0 : 2 : 1–4 : 2 : 1), the mass ratio of CCAL to PPy (1 : 0.07–1 : 0.7), PPy polymerization temperature (10–60 °C) and polymerization time (3–24 h) were investigated systematically. Besides, the experimental parameters of the adsorption process, including dosage of adsorbent (0.05–1.5 g L^{-1}), initial concentration of Cr(VI) (20–125 mg L^{-1}), pH (2–11), and co-existing anions (CO$_3^{2-}$, Cl$^-$, NO$_3^-$) were studied. The samples were taken at a predetermined interval and filtered through a 0.22 μm filter membrane. The Cr(VI) concentration was analyzed using a UV-visible spectrometer (Inesa-L5S, Shanghai Yidian Scientific Instrument Co., LTD, China) at 540 nm.[35] The Cr(VI) removal rate ($R\%$) and adsorption capacity (q_t) are determined according to the equations (eqn (1) and (2)).

$$R\% = \frac{C_0 - C_t}{C_0} \times 100\% \tag{1}$$

$$q_t = \frac{(C_0 - C_t) \times V}{m} \tag{2}$$

where C_0, C_t is the concentration of Cr(VI) at initial and a given time (t) in mg L^{-1}, V is the volume of the solution in liters, and m is the mass of the adsorbent in grams.

2.5 Adsorption isotherms

Isothermal adsorption experiments were conducted with different initial concentrations of Cr(VI) (18–685 mg L^{-1}) at 25 °C until equilibrium was obtained. Langmuir and Freundlich models, shown in eqn (3) and (4) used to fit the adsorption processes.[36]

$$q_e = \frac{Q_{max}bC_e}{1 + bC_e} \tag{3}$$

$$q_e = K_f C_e^{1/n} \tag{4}$$

where, C_e indicates the equilibrium concentration of Cr(VI). Q_{max} (mg g^{-1}) is the monolayer maximum capacity of the Langmuir model, and b is the Langmuir constant (L mg^{-1}). K_f and n are the Freundlich adsorption capacity ((mg g^{-1})/(mg L^{-1})$^{1/n}$) and Freundlich constant, respectively.

Besides, the dimensionless separation factor R_L, represented in eqn (5), is a fundamental feature of the Langmuir model and is used to determine the benefit of the adsorption process.

$$R_L = \frac{1}{1 + bC_0} \tag{5}$$

where, R_L values represent different adsorption processes, irreversible adsorption ($R_L = 0$), favorable adsorption ($0 < R_L < 1$), linear adsorption ($R_L = 1$), or unfavorable adsorption ($R_L > 1$).[37]

2.6 Adsorption kinetics

Pseudo-first-order (PFO), pseudo-second-order and Avrami fractional-order (AFO) models are used to fit the experimental data, and the coefficients and related parameters are calculated according to the following eqn (6)–(8):

$$q_t = q_e(1 - e^{-k_1 t}) \tag{6}$$

$$q_t = \frac{q_e^2 k_2 t}{1 + q_e k_2 t} \tag{7}$$

$$q_t = q_e[1 - e^{-(k_{AV}t)^n}] \tag{8}$$

where, q_t is the adsorption capacity at a given time (mg g^{-1}), k_1 (min^{-1}) belongs to the coefficient of PFO, and k_2 (g (mg^{-1} min^{-1})) is the rate coefficient of PSO. k_{AV} (min^{-1}) and n represent the corresponding rate constant and Avrami fractional adsorption order related to the adsorbed species at the active sites, respectively.

2.7 Adsorption thermodynamics

Adsorption thermodynamic parameters, such as standard free energy change (ΔG), enthalpy change (ΔH), and entropy change (ΔS) are obtained from eqn (9).[38]

$$\ln K_d = \ln \frac{Q_e}{C_e} = \frac{\Delta S}{R} - \frac{\Delta H}{RT} = -\frac{\Delta G}{RT} \tag{9}$$

where, K_d is the distribution coefficient, Q_e (mg g^{-1}) and C_e (mg g^{-1}) are the adsorption capacity of Cr(VI) on the adsorbent and its equilibrium concentrations, respectively. T is the Kelvin absolute temperature, and R is the gas constant with a value of 8.314 J mol^{-1} K^{-1}.

2.8 Batch desorption experiments

To achieve the efficient recycling of adsorbent, the regeneration and reusability of CCALP were studied according to the literature.[2] After the adsorption experiment, the adsorbent was recovered and desorbed in 20 mL 1 M NaOH solution for 1.5 h. The extracted Cr(VI) concentration was filtered and analyzed. The recovered CCALP was added to 20 mL 2 M HCl solution to vibrate for 1.5 h to regenerate the adsorption sites. After that, it was separated and dried in a vacuum oven at 60 °C for 24 h. The obtained CCALP was reused in the following adsorption cycle under the same adsorption conditions five times to evaluate their reusability. In particular, the obtained experimental results were compared with the adsorbent without desorption and regeneration.

2.9 Theoretical computations

The interaction of Cr(VI) and Cr(III) ions on the adsorbents was investigated by density functional theory (DFT) calculations with MS2019 software. The adsorption energy (E_{ads}) was calculated, and the geometry was optimized using GGA-BLYP in the DMol3 function. The spin was used due to the existence of metal. The convergence energy was set to 1×10^{-6} Ha, 500 cycles, and the optimal convergence criterion was defaulted for

other parameters. To investigate the effect of PPy on Cr(VI) adsorption, the E_{ads} of Cr(VI) ions on PPy was determined using the simulation derivation method. All the E_{ads} was calculated as follows:

$$E_{ads} = E_{tot} - (E_{sub} + E_{mol}) \tag{10}$$

where, E_{tot}, E_{sub} and E_{mol} depicted the total energy of the adsorption complex, the substrate and the isolated adsorbed molecules, respectively.

Besides, the ESP obtained by the DMol3 program in the Materials Studio 2019 software package was used to explore the interaction between Cr(VI) and prepared adsorbents.

3 Results and discussion

3.1 Microstructure characterization of adsorbents

As shown in Fig. 1a and b, irregular massive structures with rough surfaces and apparent layer-overlapping morphology were observed on the surface of the CAL and CCAL, consistent with the typical crystal morphologies of LDH materials.[39] After the polymerization of PPy on the surface of CAL, the large lamellar structure completely disappeared, forming abundant small and aggregated irregular sheet-like structures instead (Fig. 1c). Compared to CALP, CCALP exhibited similar structures with smaller particles with an average size of about 160.99 nm (Fig. 1d). Mainly because the PPy homopolymers were in the form of nearly spherical particles, and most of the

LDHs surface was effectively wrapped by PPy, causing the layered structures of CAL and CCAL to be damaged. According to the EDS analysis (Fig. 1e), the Co, Ca, Al, and N were uniformly distributed on the surface of CCALP, indicating that the CCALP was successfully modified by Co and PPy, and the content of Co was relatively low (Fig. 1f).

XRD analysis was conducted to investigate the crystal structure of CAL, CCAL, CALP and CCALP (Fig. 2a). Distinct diffraction peaks were observed at about 10°, 20.2°, 31.6°, 41.9° of CAL and CCAL, belonging to the (003), (006), (110), (206) crystal planes of LDHs (PDF#50-0652).[34] However, the intensity of CCAL slightly decreased with Co doping, suggesting that Co doping may affect the cationic layer structure of LDHs. The absence of characteristic diffraction peaks of Co may be due to its low content. However, the presence of Co in CCAL could be confirmed by other characterization methods, which will be discussed in detail later. After doping with PPy, most of the characteristic peak intensities of LDHs decreased, indicating increased disorder in the layer stacking and poor crystallinity.[40,41] In contrast, a broad peak appeared in the range of $2\theta = 10-25°$, corresponding to a shift of the $\pi-\pi$ interaction of the amorphous PPy chains,[34] indicating that the polymer matrix was decorated on the surface of CCALP. The introduction of PPy resulted in poor crystallinity of LDHs while promoting increased diffraction peak intensity of $Al(OH)_3$ at 38.26° in CALP and CCALP.

Fig. 2b exhibits the ATR-FTIR spectra of the above four adsorbents. The absorption peaks of CCALP at about 786 cm^{-1}
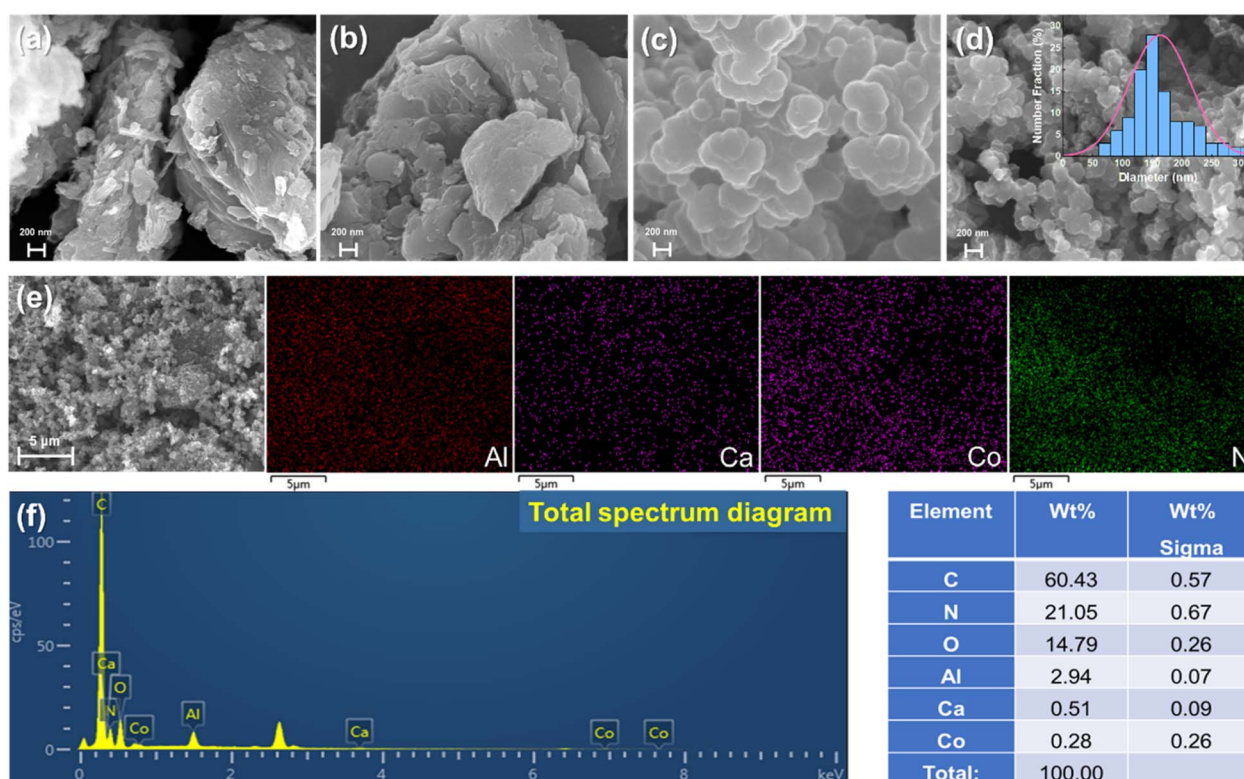

Fig. 1 SEM images of (a) CAL, (b) CCAL, (c) CALP and (d) CCALP. (e) EDS mapping of Al, Ca, Co and N in CCALP. (f) Total spectrum and table of element content of the CCALP.
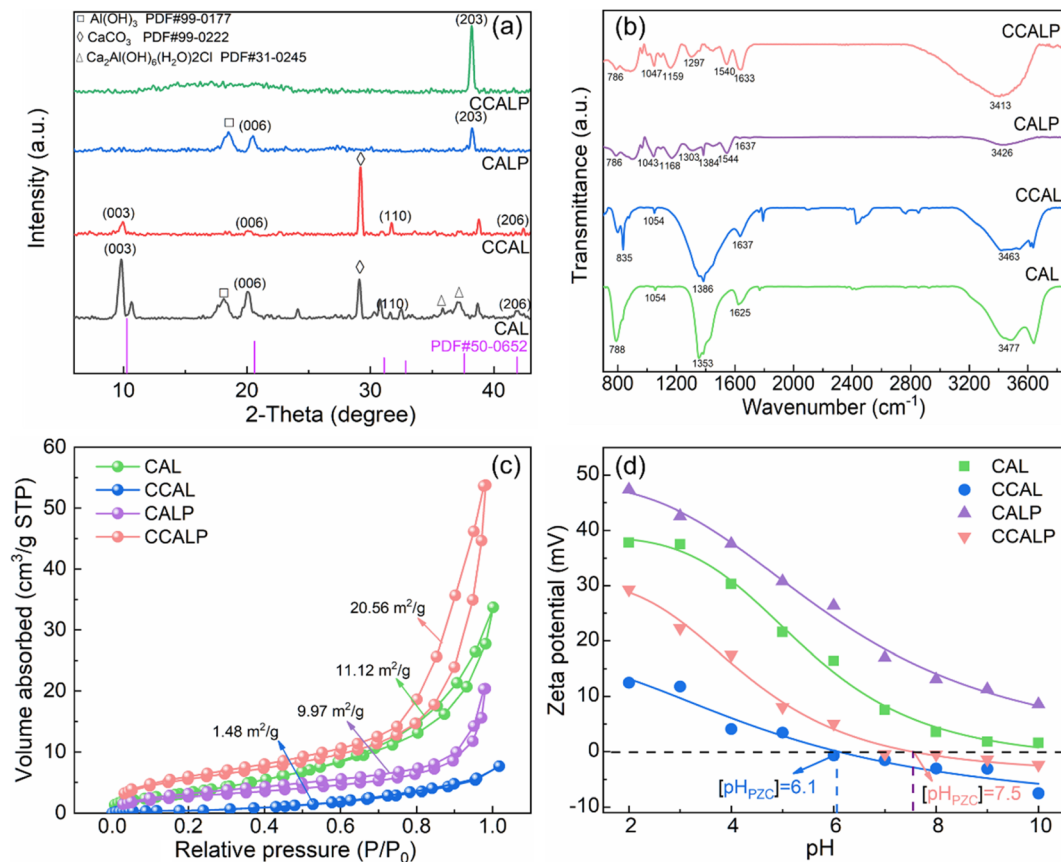
Element	Wt%	Wt% Sigma
C	60.43	0.57
N	21.05	0.67
O	14.79	0.26
Al	2.94	0.07
Ca	0.51	0.09
Co	0.28	0.26
Total:	100.00	

Fig. 2 (a) XRD patterns, (b) ATR-FTIR spectra, (c) N_2 adsorption–desorption isotherms (d) zeta potential, of CAL, CCAL, CALP and CCALP.

and 1047 cm^{-1} referred to the Al–O bending vibration and Ca–O vibration, respectively,[42] indicating the persistence of the original LDHs structure even after the co-modification by Co and PPy. Bands at 3200–3700 cm^{-1} were related to the O–H stretching vibration, and the band at 1625 cm^{-1} was associated with the angular deformation of water molecules.[43,44] For CALP and CCALP, new characteristic bands appeared around 1540 cm^{-1}, associated with C=C and imine stretching vibrations.[45] The peaks at 1297 cm^{-1}, 1159 cm^{-1} and 1047 cm^{-1}, correspond to C–N stretch vibration, C–N bond in-plane deformation vibration, and C–H bond plane vibration, respectively.[34] These observations confirmed the successful intercalation of PPy in LDHs. Compared to CALP, the peak intensity increased slightly in CCALP, indicating that the Co doping promoted the coating efficiency of PPy on its surface.

N_2 adsorption–desorption isotherms of the adsorbents in Fig. 2c indicated that they all exhibited type IV isotherms with H3-type hysteresis loops, suggesting typical mesoporous structures.[46,47] Normally, the type H3 ring is associated with non-rigid aggregates of plate-like particles, consistent with the layered structure of the LDHs.[46] The average pore diameters of the materials were all within the range of 2–50 nm (Table S1†), further suggesting the presence of mesopore structures. Due to the aggregation of PPy chains, CALP presented the smallest pore diameter, while it was mitigated by simultaneously Co doping. The decline in the specific surface area of CCAL

indicated that the doping of Co may result in changes in the LDHs layer spacing and void structure, thus affecting the material's microstructure. Among all the samples, the CCALP demonstrated the maximum surface area (20.56 m^2 g^{-1}) and pore volume (0.0810 cm^3 g^{-1}) due to the successful PPy modification, offering an abundance of active sites for Cr(vɪ) removal.

The electrostatic adsorption ability of the adsorbent was determined by zeta potential.[48,49] Compared to CAL, the point of zero charge (pH$_{pzc}$) of CCAL significantly decreased to 6.1. It is attributed to Co^{2+} ions substituting some Ca^{2+} ions in CAL, and Co^{2+} has a smaller radius than Ca^{2+}, leading to an increase in charge density between the LDH layers and a decrease in the positive charge of the LDHs surface. In addition, the positively charged Co may interact with the anions present between the LDH layers, thereby reducing the pH$_{pzc}$ of the material. The pH$_{pzc}$ of CALP sharply increased since PPy is a conductive polymer with a high positive charge density, affecting the surface charge distribution of LDH. The pH$_{pzc}$ of CCALP was 7.5. When the pH of the solution was below this value, the zeta potential of the adsorbent was positive, benefiting the adsorption of Cr(vɪ) (in the form of HCrO$_4^-$ or Cr$_2$O$_7^{2-}$) anions by electrostatic attraction. Conversely, the deprotonation of the adsorbent surface and the electrostatic repulsion effect reduced the adsorption rate of Cr(vɪ).[50] In addition, under alkaline conditions, OH$^-$ may compete with Cr(vɪ) for adsorption sites, which was not conducive to Cr(vɪ) adsorption.

3.2 Adsorption performance of CCALP

3.2.1 Optimization of experimental conditions. The preparation process parameters, including the molar ratio of Co : Ca : Al, the mass ratio of CCAL : PPy, polymerization time and temperature significantly affect the Cr(VI) adsorption performance of CCALP. As shown in Fig. 3a, the adsorption efficiency of Cr(VI) on CCAL dramatically increased and then decreased with increasing the doped Co content. Because an excessive amount of Co destroyed the layer structure of the CCAL, forming large, tightly packed structures instead (Fig. S1†). Even at the optimal molar ratio of Co : Ca : Al = 1 : 2 : 1, only 15 mg g^{-1} adsorption capacity and 37.5% removal efficiency of Cr(VI) were obtained at 10 min. This situation was not effectively alleviated, even with an extended adsorption time of 2 hours (Fig. S2†). This indicated that Co doping alone did not substantially enhance the Cr(VI) adsorption efficiency of CCAL, primarily due to the diminished surface area (Fig. 2c) and the limited number of active sites. While Co exhibits some catalytic activity, its electron transfer capability is insufficient to improve the reduction efficiency of Cr(VI).

However, the Cr(VI) adsorption performance was remarkably improved after PPy doping, with about 39.53 ± 0.4 mg g^{-1} adsorption capacity and 98.83 ± 1.0% removal efficiency at a mass ratio of CCAL : PPy = 1 : 0.35 (Fig. 3b). Mainly because the pyrrole nitrogen group on the CCAL surface participated in the binding, adsorption and reduction of Cr(VI) in aqueous solution.[51] Thus, increasing the PPy doping amount enhanced the number of adsorption sites and improved the adsorption efficiency. As shown in Fig. 3c and d, the low polymerization temperature (<30 °C) and short time (<6 h) during the preparation of CCALP were not conducive to the formation of well-structured and highly efficient PPy. Since PPy is formed by *in situ* polymerization, triggered by the oxidant FeCl$_3$, both temperature and time are critical parameters that significantly influence the chain growth and overall polymer structure.[34] However, excessively increasing the polymerization temperature (60 °C) or extending the polymerization time (24 h) led to the formation of agglomerated CCALP masses (Fig. S3†), which totally damaged the layered structure and reduced the adsorption surface area.

3.2.2 Comparison of adsorption performance between CCAL and CCALP under different conditions. The adsorbent dosage had a vital effect on the Cr(VI) adsorption performance. When the concentration of CCALP increased from 0.25 g L^{-1} to 0.5 g L^{-1}, the adsorption capacity and efficiency of Cr(VI) increased by 15.4 mg g^{-1} and 70%, respectively (Fig. 4a). As the adsorbent dosage increased, the total surface area of the adsorbent was also enhanced, and more adsorption sites were available, allowing more Cr(VI) ions to be captured and immobilized. Besides, a high concentration gradient could be maintained by increasing the amount of CCALP, which facilitated the transfer and diffusion of Cr(VI) ions to the surface of the adsorbent. However, further increasing the concentration to 1.0 g L^{-1} resulted in a significant decrease in adsorption capacity while the adsorption efficiency remained constant. For
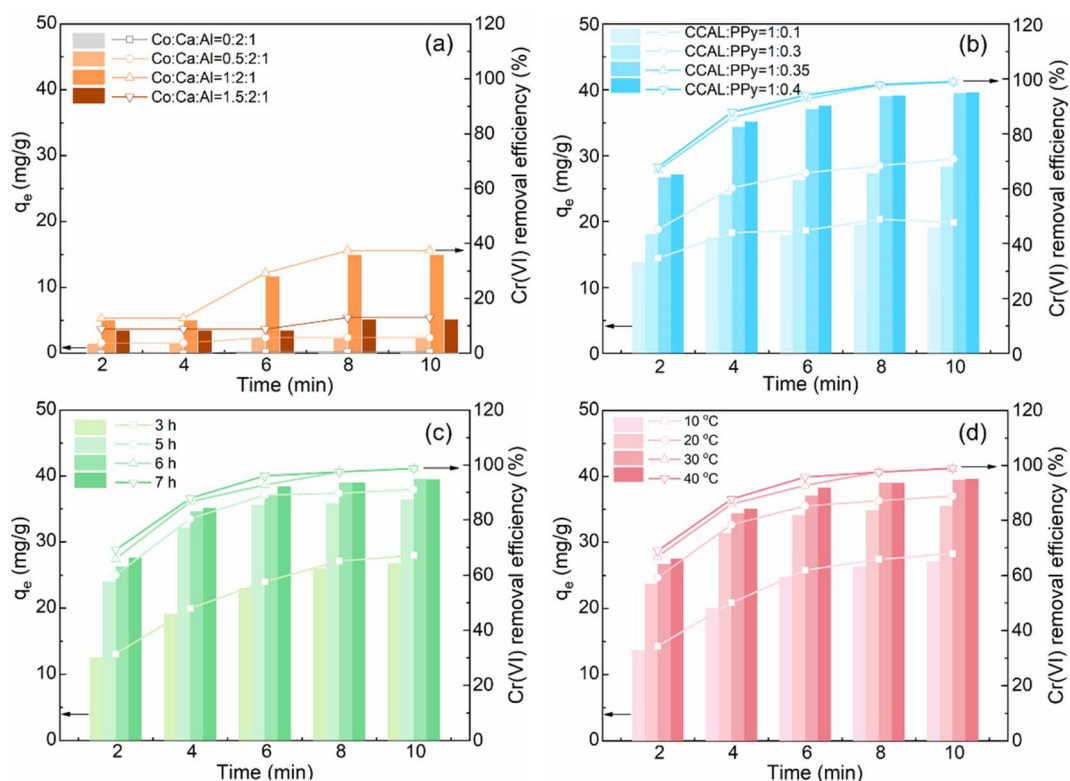

Fig. 3 Effects of (a) molar ratio of Co : Ca : Al, (b) mass ratio of CCAL : PPy, (c) polymerization time, (d) polymerization temperature of CCALP on the adsorption capacity and efficiency of Cr(VI).
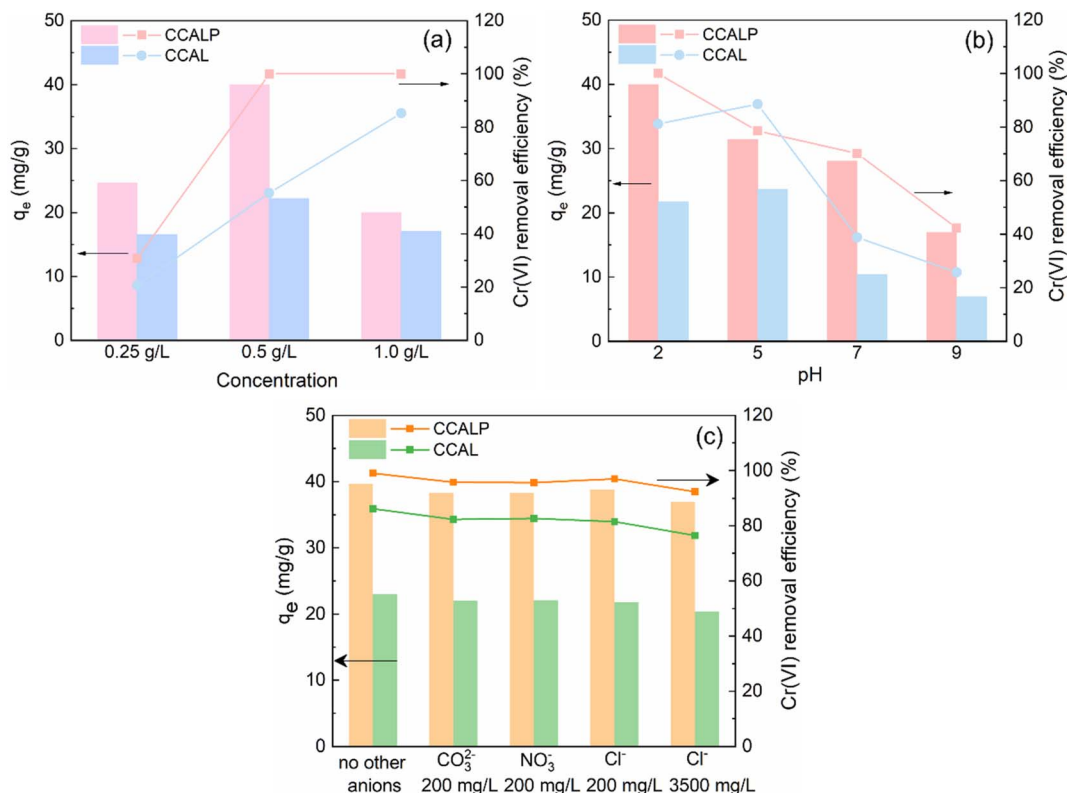
Fig. 4 Comparison of effect of (a) dosage of adsorbent, (b) pH, (c) coexisting anions on the adsorption capacity and efficiency of Cr(VI) by CCAL and CCALP.

0.25 g L^{-1} CCALP, approximately 100% removal efficiency of Cr(VI) was obtained by extending the adsorption time to 160 min (Fig. S4†). However, excessively long adsorption times are not practical. For CCAL, even at the optimized concentration, its adsorption capacity of Cr(VI) was only half of that of CCALP, which indicated that the doping of PPy played a decisive role in the removal of Cr(VI) by CCALP, which will be explained in detail in the mechanism section.

In general, the initial pH of the solution significantly affects the charge distribution on the adsorbent surface and the Cr(VI) species in the aqueous solution. As shown in Fig. 4b, the optimized pH of CCAL was 5, which was higher than that of the CCALP, meaning at low pH (pH = 2), the surface of the CCAL may carry more positive charges, resulting in enhanced electrostatic repulsion and reduced adsorption efficiency. However, the highest adsorption capacity and efficiency of Cr(VI) on CCALP were obtained at pH 2. CCALP could better adapt to the acidic environment due to the excellent chemical stability of the PPy, which can protect the LDH material from acid corrosion. Besides, in the pH range of 1–5, Cr(VI) primarily exists in forms such as HCrO$_4^-$, which occupy fewer active sites and require the least adsorption free energy.[52] Additionally, the pH$_{pzc}$ of CCAL and CCALP was 6.1 and 7.5, respectively. When pH < pH$_{pzc}$, the surface of adsorbents was positively charged, facilitating the adsorption of negatively charged Cr(VI), and *vice versa*. Moreover, the high redox potential of Cr(VI) (approximately 1.33 eV) enhances its reduction at low pH,[53] thereby improving the removal efficiency of Cr(VI).

Anions, such as CO$_3^{2-}$, Cl$^-$ and NO$_3^-$ in actual wastewater may have competitive adsorption reactions with Cr(VI). Therefore, the influence of coexisting anions on the adsorption of Cr(VI) by CCAL and CCALP was systematically evaluated under optimal adsorption conditions. Notably, CO$_3^{2-}$ can undergo hydrolysis in aqueous solutions to form OH$^-$, which may subsequently diminish the removal efficiency of Cr(VI).[54] As illustrated in Fig. 4c, the addition of 200 mg L^{-1} CO$_3^{2-}$, Cl$^-$ or NO$_3^-$ ions resulted in a reduction of the adsorption capacity and efficiency by 0.83–1.36 mg g^{-1} and 2.07–7.09%, respectively. Despite the high concentration of Cl$^-$ (3500 mg L^{-1}) in raw tannery wastewater,[55] the CCALP showed excellent selectivity for Cr(VI) due to the strong interaction forces between Cr(VI) and the adsorbent sites, resulting in 92.38% removal efficiency of Cr(VI), suggesting that coexisting ions exerted a negligible effect on the adsorption process of CCAL and CCALP.

3.2.3 Adsorption isotherms analysis. The Langmuir and Freundlich isotherm models were used to simulate the experimental results of Cr(VI) adsorption by CAL, CCAL, CALP and CCALP at different temperatures presented in Fig. 5. By comparing the determination coefficient (R^2) of the two models, it was found that the Langmuir model more accurately described the experimental data. This indicated that the adsorption of Cr(VI) on the four adsorbents followed the monolayer adsorption hypothesis, suggesting that the adsorption sites on the adsorbent surface were equivalent and did not influence each other. As shown in Table S2,† the maximum
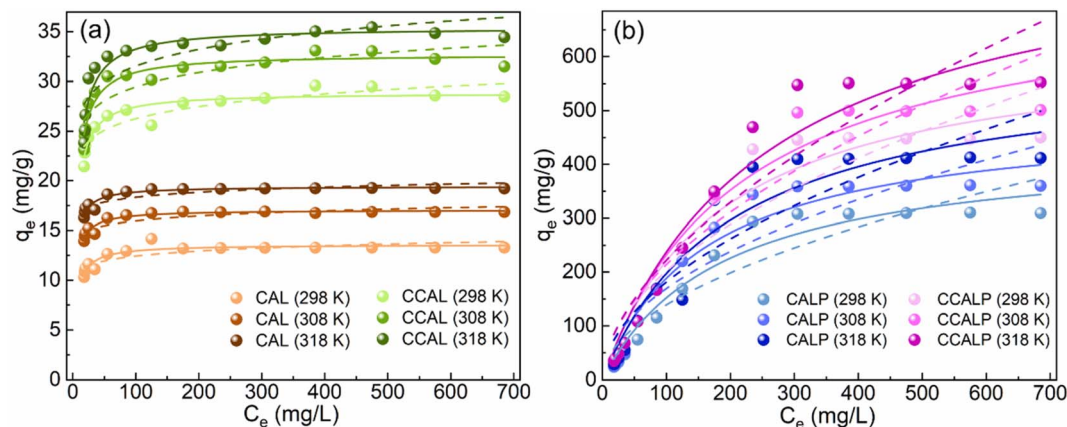
Fig. 5 Langmuir (solid line) and Freundlich models (dashed line) for Cr(VI) adsorption on (a) CAL and CCAL, (b) CALP and CCALP.

adsorption capacity (Q_{max}) of all adsorbents increased significantly with increasing temperature from 298 K to 318 K, which may be due to the increased thermal energy of the adsorbents.[56] Specifically, at 318 K, the maximum adsorption capacity of CAL was 19.42 mg g^{-1}, which increased to 35.44 mg g^{-1} for CCAL, indicating that Co doping enhanced its adsorption capacity. The Q_{max} of Cr(VI) on CALP and CCALP increased to 594.64 mg g^{-1} and 845.25 mg g^{-1}, respectively, mainly because PPy provided more functional groups and adsorption sites for Cr(VI) capture. Besides, the R_L values were between 0 and 1 (Table S2†), indicating favorable adsorption of Cr(VI) on all adsorbents. Compared to other reported modified LDHs (Table 1), the high removal efficiency of Cr(VI) with a low CCALP dosage in a short time demonstrated its superior application potential under similar operating conditions.

3.2.4 Adsorption thermodynamics analysis. Temperature influences the thermal motion of molecules and plays a crucial role in the adsorption process. For CAL, the positive ΔG and negative values at various temperatures indicated that Cr(VI) adsorption was non-spontaneous and ordered, explaining the low adsorption efficiency of Cr(VI) on CAL under standard conditions (Table 2). The negative values of ΔG and ΔH for the other three adsorbents indicated that the adsorption of Cr(VI) was spontaneous and exothermic. The ΔG value of CCAL and CALP increased with rising temperature, confirming the spontaneous improvement of Cr(VI) adsorption by increasing the thermal energy. This was because the increase in temperature

could reduce the viscosity of the solution, promote the diffusion of pollutant molecules through the internal pores of the adsorbent, and increase the active sites by forming internal bonds.[60] With the simultaneous introduction of Co and PPy into CCALP, the highest ΔG value of −2.5965 kJ mol^{-1} was obtained at 318 K, attributed to the enlarged pore size and surface

Table 2 Thermodynamic parameters of Cr(VI) adsorption by four adsorbents at different temperatures

Adsorbents	T (K)	$\ln K_d$	ΔG (kJ mol^{-1})	ΔH (kJ mol^{-1})	ΔS (J mol^{-1} K^{-1})
CAL	288	−0.9416	2.2546	−1.508	−12.862
	298	−0.8916	2.2090		
	308	−0.9676	2.4777		
	318	−0.9943	2.6287		
CCAL	288	0.2390	−0.5723	−0.464	0.333
	298	0.2231	−0.5529		
	308	0.2151	−0.5508		
	318	0.2151	−0.5687		
CALP	288	0.5710	−1.3672	−3.889	−8.896
	298	0.5008	−1.2407		
	308	0.4318	−1.1057		
	318	0.3716	−0.9824		
CCALP	288	1.0080	−2.4135	−0.708	5.903
	298	1.0080	−2.4973		
	308	0.9746	−2.4956		
	318	0.9821	−2.5965		

Table 1 Comparison of removal efficiency of Cr(VI) on various LDHs

| Adsorbents	Cr(VI) concentration (mM)	Operating conditions	Adsorbent dosage (g L^{-1})	Removal efficiency	Ref.
PANI/LDH@MMt	0.170	T = 25 °C; pH = 2	1.00	99% (120 min)	57
Fe$_3$O$_4$@LDH	0.170	T = 25 °C; pH = 5	1.00	100% (30 min)	21
ZnMgAl LDH-algae composites	0.170	T = 30 °C; pH = 4	0.30	99% (70 min)	58
CoMgAl-LDH	0.068	T = 25 °C; pH = 5	0.50	95% (60 min)	3
LDH-EDTA	0.170	T = 25 °C; pH = 3–10	1.50	96% (60 min)	59
CAL	0.170	T = 25 °C; pH = 5–6	1.47	100% (180 min)	34
CAL-PPy	0.340	T = 25 °C; pH = 2	1.51	100% (180 min)	
CCALP	0.068	T = 25 °C; pH = 2	0.50	98.83% (10 min)	This study
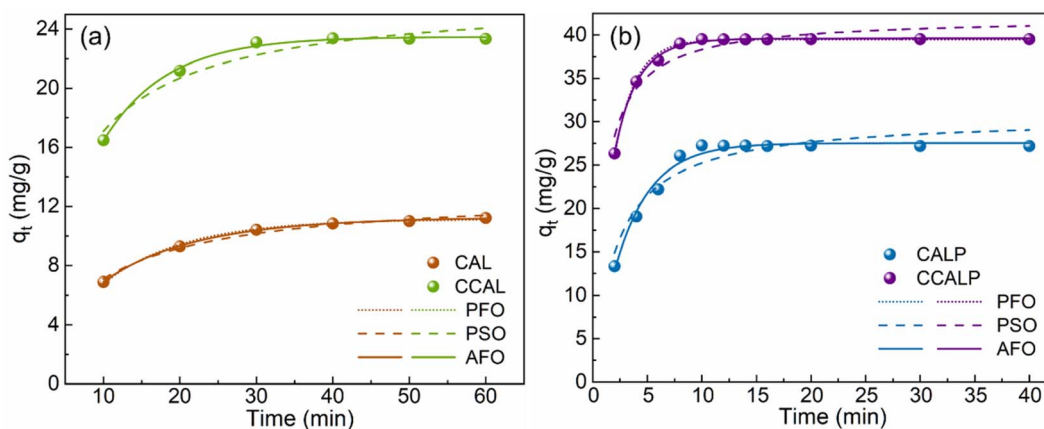
Fig. 6 Adsorption kinetics of Cr(vi) in static adsorption process by (a) CAL and CCAL, (b) CALP and CCALP.

activation of CCALP. For CCAL and CCALP, positive ΔS values indicated increased disorder and randomness at the solid–liquid interface during Cr(vi) adsorption.[34,36]

3.2.5 Adsorption dynamics analysis. Adsorption dynamics is a crucial theory for understanding the dynamic equilibrium between adsorption rate and capacity. As illustrated in Fig. 6, the adsorption capacity of the four adsorbents increased rapidly and then plateaued as the number of available adsorption sites decreased, reaching equilibrium. Compared to CAL and CCAL, CALP and CCALP achieved adsorption equilibrium more quickly and exhibited excellent adsorption capacity. The PFO, PSO and AFO models were employed to fit the Cr(vi) adsorption kinetic data. Compared to the others, the PFO model fitted well for the CCAL and CALP, indicating that the adsorption processes were controlled by liquid film diffusion. The adsorption of Cr(vi) by CCALP was better described by the AFO model, reflecting the complexity and multiple kinetic stages involved in Cr(vi) adsorption. Notably, the adsorption rate constant for CCALP was 5.9 times higher than that of CAL, indicating that CCALP possessed more surface adsorption sites and facilitated easier interaction with Cr(vi) (Table 3).

3.3 Adsorption mechanism

To explore the adsorption mechanism of Cr(vi) on CCALP, XRD, ATR-FTIR and XPS spectra before and after Cr(vi) adsorption were studied. Compared to Fig. 2a, a new series of characteristic diffraction peaks of $(CaCrO_4 \cdot 2H_2O)$[59] appeared in CAL and CCAL with high peak intensity after Cr(vi) adsorption (Fig. 7a). This is probably due to the ion exchange between Cr(vi) ions and NO_3^- ions in the interlayer of the LDHs. Additionally, a new absorption peak appeared at 879 cm^{-1} on CAL and CCAL after Cr(vi) adsorption, corresponding to the tensile vibration of the Cr–O bond, suggesting that the adsorption process altered the local environment of Cr(vi) (Fig. 7b). However, these peaks were not found in the XRD and ATR-FTIR patterns of CALP and CCALP, suggesting the Cr(vi) removal mechanism may not only be ion exchange. As shown in Fig. 7c, a rapid decrease in the pH_{pzc} of the four absorbents was observed, especially for CCAL and CCALP, where the pH_{pzc} decreased to approximately 4.29 and 5.6, respectively. This was primarily due to the accumulation of a large amount of Cr(vi) on the surface of the materials, indicating a strong electrostatic interaction between Cr(vi) and the absorbents. In addition, the changed morphology and structure (Fig. 1d) might affect their interaction with Cr(vi), preventing the changes in adsorption peaks.

Fig. 8a and b illustrated that the binding energy of Co 2p$_{3/2}$ and Co 2p$_{1/2}$ for CCAL and CCALP shifted positively after Cr(vi) adsorption, indicating that the charge transfer between Cr(vi) and Co could increase the ratio of Co(iii), promoting the electrostatic adsorption of Cr(vi). Since PPy and Co(ii) can reduce

Table 3 Kinetic modeling of Cr(vi) adsorption by CAL, CCAL, CALP and CCALP adsorbents and their corresponding parameters

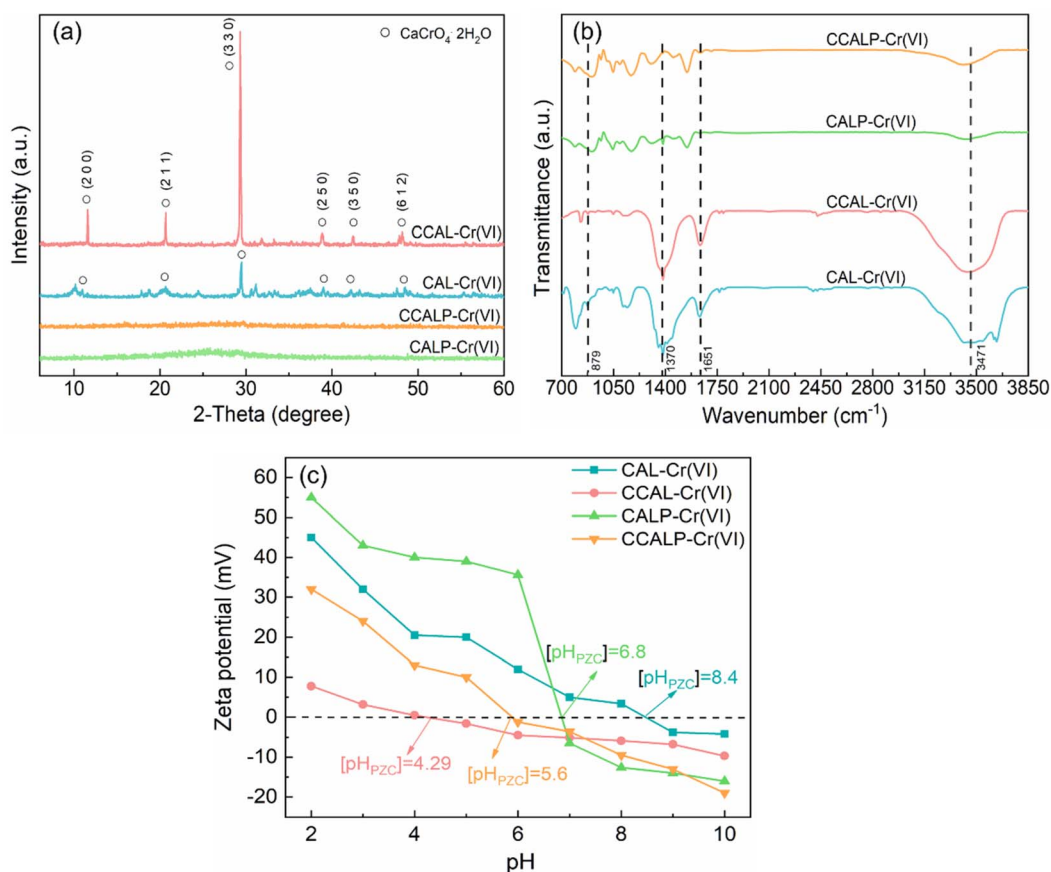| Kinetic models	Kinetic parameters	Adsorbents			
		CAL	CCAL	CALP	CCALP
PFO	R^2	0.995	0.996	0.980	0.994
	q_e (mg g^{-1})	11.14	23.49	27.53	39.47
	k_1 (min^{-1})	0.0938	0.1204	0.3123	0.5365
PSO	R^2	0.984	0.932	0.904	0.907
	q_e (mg g^{-1})	12.97	26.21	30.58	42.04
	k_2 (g mg^{-1} min^{-1})	0.0093	0.0071	0.0154	0.0245
AFO	R^2	0.999	0.994	0.978	0.997
	q_e (mg g^{-1})	11.29	23.48	27.52	39.60
	k_{AV} (min^{-1})	0.0937	0.1203	0.3122	0.5530
	n	0.8918	1.0037	1.0029	0.9064

Fig. 7 (a) XRD patterns, (b) ATR-FTIR spectra, (c) zeta potential of CAL, CCAL, CALP and CCALP after Cr(vi) adsorption.

some of Cr(vi) to Cr(iii), thereby increasing the removal capacity of Cr(vi). In fact, after Cr(vi) adsorption, the ratio of Co(ii) decreased by 3.04% and 7.45% for CCAL and CCALP, respectively, suggesting that Co(ii) participated in the reduction of Cr(vi), with this effect being amplified in the presence of PPy. As shown in Fig. 8c and d, the N 1s in CALP and CCALP mainly
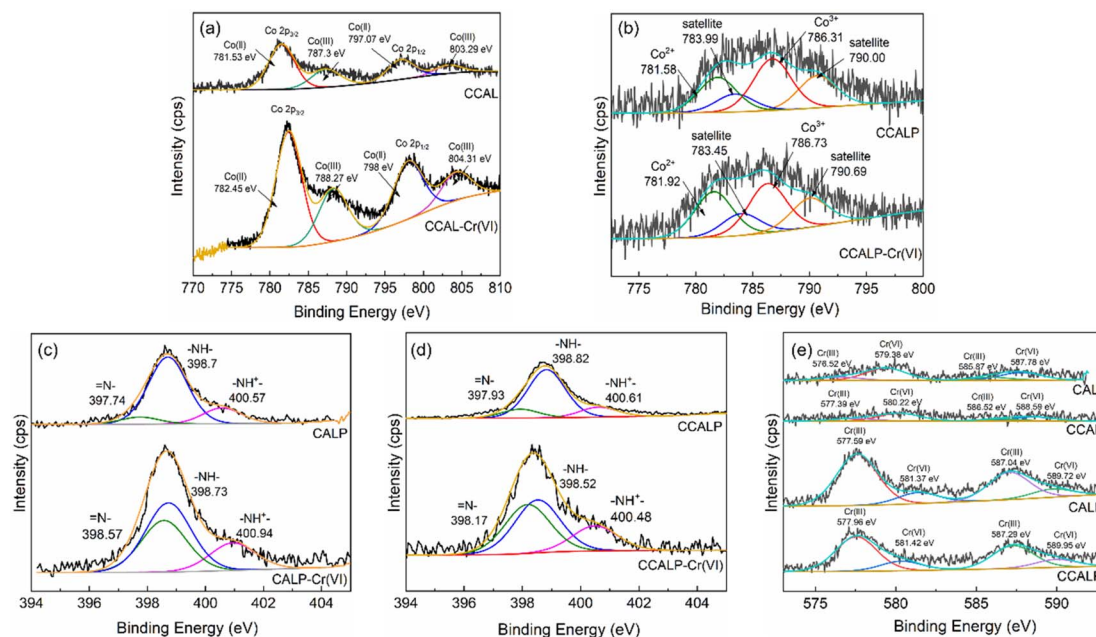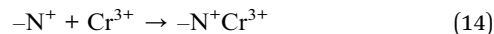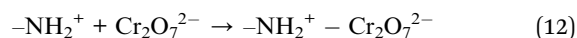

Fig. 8 XPS spectra of Co 2p of (a) CCAL and (b) CCALP before and after Cr(vi) adsorption; N 1s of (c) CALP and (d) CCALP before and after Cr(vi) adsorption; (e) Cr 2p of the four adsorbents after Cr(vi) adsorption.

exist in the forms –NH–, –NH$^+$– and =N–. After Cr(vi) adsorption, the content of =N– was increased by 25.42% for CCALP, implying that –NH– lost electrons and converted to =N–, reducing Cr(vi) to Cr(iii) (eqn (11)–(13)). As it was confirmed in Fig. S5,† the percentage of Cr(iii) on CLAP and CCALP was about 14.29% and 16.15%, respectively. However, the ratio of Cr(iii) on CAL and CCAL was negligible, indicating the more efficient reduction ability of PPy than Co(ii). The deprotonated pyrrole N can adsorb Cr(iii) through the Cr(iii)–N covalent bond to form a complex[61] (eqn (14)). After adsorption, Cr 2p peaks corresponding to Cr(vi) and Cr(iii) were observed on the surface of the four adsorbents (Fig. 8e), confirming the multiple removal mechanism of Cr(vi).

$$-NH_2^+ + HCrO_4^- \rightarrow -NH_2^+ - HCrO_4^- \quad (11)$$

$$-NH_2^+ + Cr_2O_7^{2-} \rightarrow -NH_2^+ - Cr_2O_7^{2-} \quad (12)$$

$$HCrO_4^- + 3PPy^0 + 7H^+ \rightarrow Cr^{3+} + 4H_2O + 3PPy^+ \quad (13)$$

$$-N^+ + Cr^{3+} \rightarrow -N^+Cr^{3+} \quad (14)$$

Moreover, DFT calculations were performed to further reveal the enhancement removal mechanism of Cr(vi) on CCALP. Firstly, the E_{ads} values were calculated to determine the bonding stability between the adsorbents and the HCrO$_4^-$ (the dominant form of Cr(vi) at the optimized pH). As shown in Fig. 9a, the E_{ads} values of HCrO$_4^-$ on the four adsorbents were negative, indicating spontaneous adsorption. Compared to CAL, the E_{ads} increased by 0.13 eV on CCAL after Co doping, and it dramatically increased to −4.50 eV after PPy doping alone, likely due to the formation of more stable complexes with HCrO$_4^-$ through π–π interaction or hydrogen bonding. After co-modification by Co and PPy, the E_{ads} of CCALP for HCrO$_4^-$ was further enhanced to −5.88 eV. Additionally, all four adsorbents exhibited high E_{ads} values for Cr$_2$O$_7^{2-}$, another form of Cr(vi), with a consistent increasing trend (Fig. S6†). This indicates that regardless of the form of Cr(vi), CCALP demonstrated the highest adsorption performance.
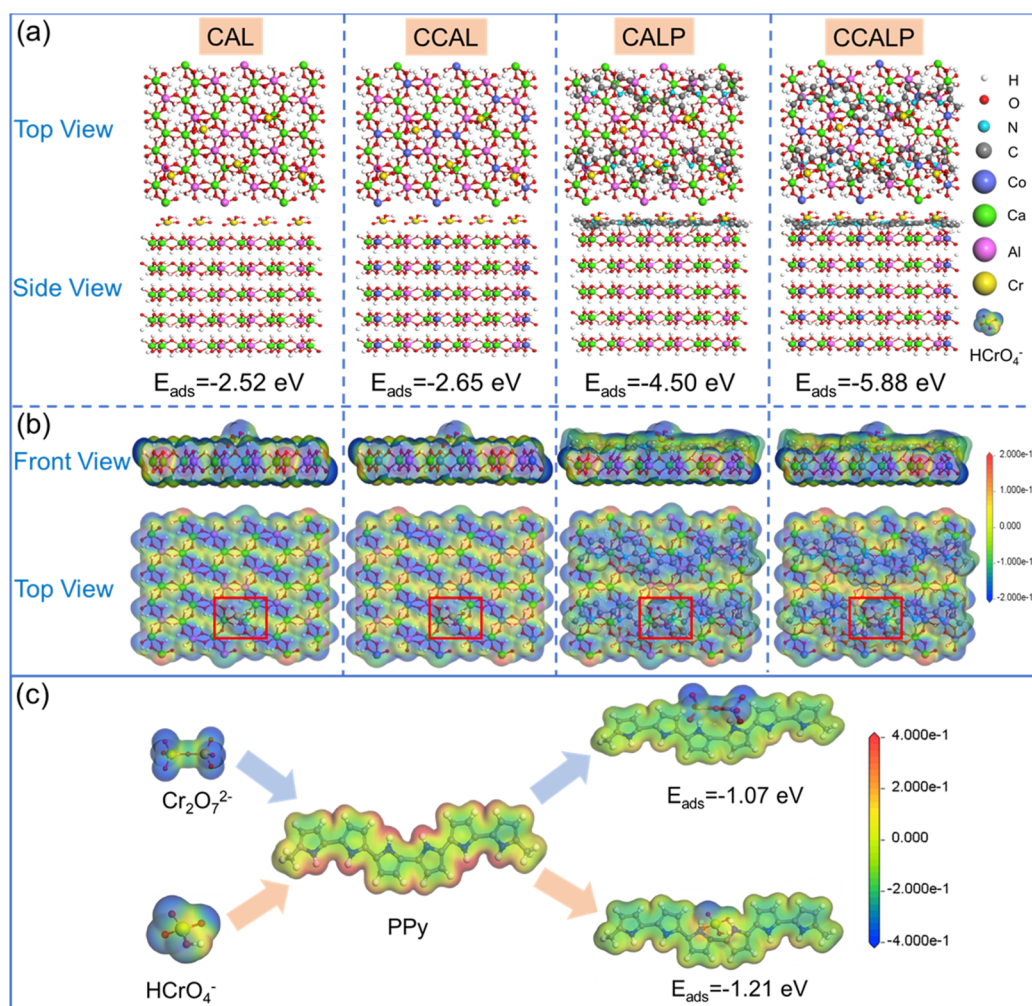

Fig. 9 (a) Top and side views of the atomic structures of CAL, CCAL, CALP and CCALP after adsorption of Cr(vi) under optimal configuration; (b) front and top views of the ESP mapping of CAL, CCAL, CALP and CCALP after Cr(vi) adsorption (inside the red box is the HCrO$_4^-$); (c) electrostatic potential mapping of Cr$_2$O$_7^{2-}$, HCrO$_4^-$, PPy monomer, PPy after Cr(vi) adsorption and the E_{ads} of the optimal configuration of PPy for Cr$_2$O$_7^{2-}$ and HCrO$_4^-$ adsorption.

To further reveal the synergistic effect of PPy and Co on Cr(VI) adsorption, ESP mapping of CAL, CCAL, CALP and CCALP after Cr(VI) adsorption was investigated (Fig. 9b). The blue area of the ESP indicates a negative electrostatic potential representing the nucleophilic group, and the red region indicates a positive electrostatic potential representing the electrophilic group. After Co modification, the electrophilic of CCAL enhanced, facilitating $HCrO_4^-$ adsorption. However, the ESP mapping of CCALP showed deepened blue regions, indicating the increase in nucleophilic with PPy doping, hindering $HCrO_4^-$ adsorption from an electrostatic perspective, which was inconsistent with the experimental results and E_{ads}. This indicated that the removal mechanism of $HCrO_4^-$ on CCALP was not dominated by electrostatic attraction. To further reveal the interaction between PPy and Cr(VI), the ESP mapping of $HCrO_4^-$, $Cr_2O_7^{2-}$, PPy monomer, and PPy after Cr(VI) adsorption was investigated. As shown in Fig. 9c, the oxygenated end of $HCrO_4^-$ and $Cr_2O_7^{2-}$ presented a highly negative electrostatic surface. In contrast, the surface of the N–H chain end on the PPy molecules showed positive electrostatic potential. Therefore, the oxygen-containing parts of the $Cr_2O_7^{2-}$ and $HCrO_4^-$ were the vital affinity sites to be adsorbed by PPy alone due to electrostatic complementation of hydrogen bonding.

Therefore, Cr(VI) adsorption on the surface of CCLAP was a complex physical and chemical adsorption process (Fig. 11).
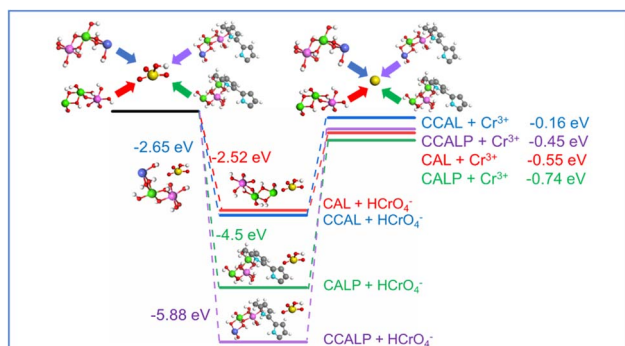

Fig. 10 The energy needed for $HCrO_4^-$ and Cr^{3+} pre-adsorbed on CAL, CCAL, CALP and CCALP.

Firstly, the introduction of Co and PPy increased the specific surface area of CaAl-LDH (Fig. 2c). The formed mesoporous structure with average pore diameters of 2–50 nm provided more adsorption sites and pores for improving the diffusion and physical adsorption capacity of Cr(VI) through van der Waals forces and electrostatic interactions. Moreover, the coexistence of Co and PPy altered the surface charge characteristics of the material, regulated the zeta potential and pH_{pzc}, and promoted the strong electrostatic interaction between Cr(VI) and the absorbents. Besides, the electrostatic interaction of Cr(VI) was stronger than that of NO_3^- and can spontaneously replace NO_3^- in the middle layer of the LDHs.[34] In addition, an ion exchange reaction may also occur between OH^- and Cr(VI), as shown in eqn (15), where M stands for Co, Ca, or Al.

$$M–OH + Cr(VI) \rightarrow OH^- + M–Cr(VI) \quad (15)$$
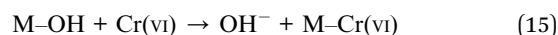
Moreover, Co ions could provide abundant surface sites that may undergo chemisorption with Cr(VI) to form stable complexes. The surface of PPy was rich in amino, hydroxyl and other functional groups, which could be chemically adsorbed with Cr(VI) to form stable chemical bonds. For example, the protonated nitrogen ($–NH_2^+$) and protonated hydroxyl group ($\equiv MOH_2^+$) on the surface of CCALP adsorbed Cr(VI) by electrostatic binding. Besides, Cr(VI) could be reduced to Cr(III) by PPy and Co(II), and adsorbed by deprotonated pyrrole N and $\equiv MOH$.[31] Therefore, the adsorption coupled mechanism of Cr(VI) included physical and chemical adsorption, such as electrostatic interaction, ion exchange, complexation and reduction.

However, compared to Cr(VI), the E_{ads} of Cr(III) on CAL, CCAL, CALP, and CCALP significantly decreased (Fig. S7† and 10). Since Cr(III) is positively charged and the LDHs have negatively charged interlayers, the ion exchange reaction could not occur. Furthermore, Cr(III) has a weaker migration ability than Cr(VI), resulting in lower contact efficiency with the adsorbent surface.

3.4 Recycling and regeneration performance of CCALP

The recycling and regeneration performance of CCALP was evaluated through five successive Cr(VI) adsorption experiments.
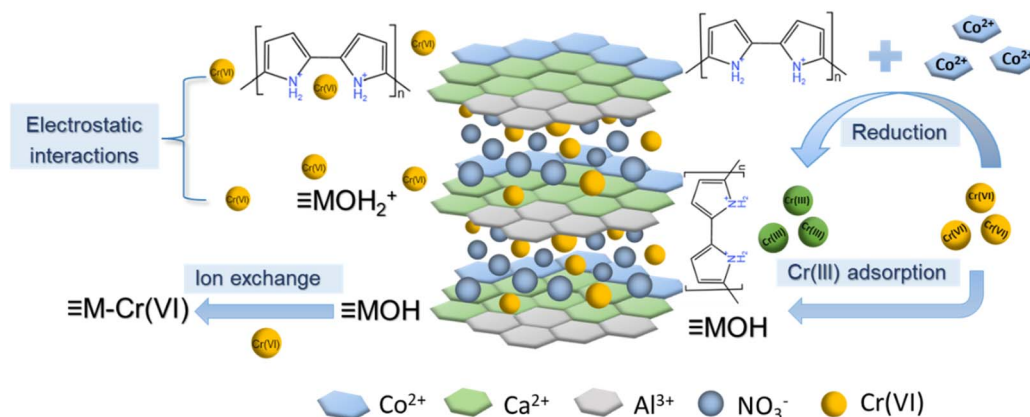

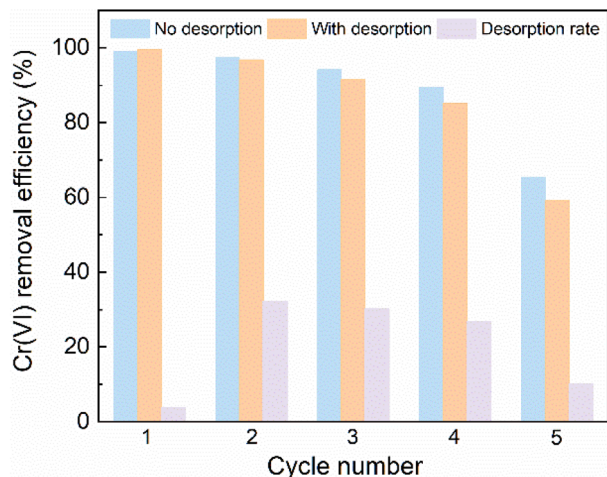Fig. 11 Proposed adsorption mechanism of Cr(VI) on CCALP.

Fig. 12 Five cycles adsorption–desorption performance of Cr(VI) on CCALP.

As shown in Fig. 12, compared with the high adsorption efficiency of Cr(VI), its desorption rate was low, primarily due to the reduction of adsorbed Cr(VI) to Cr(III), as confirmed by the XPS analysis (Fig. 7e). After treatment by 2 M HCl, the chromium species were released, regenerating the adsorption sites for the next cycle. About 90% Cr(VI) removal efficiency was maintained in the first four cycles but dropped significantly by 25.98% in the fifth cycle. This decrease is likely due to the high concentration of HCl used in the desorption process, which may accelerate the decomposition of PPy in CCALP, thereby affecting its reduction ability. Notably, the Cr(VI) removal rate on CCALP without any regenerative treatment was better than that of CCALP after desorption in the five recycles, indicating that the reduction of Cr(III) was dominant during the adsorption of Cr(VI) by CCALP.

4 Conclusion

In this study, Co and PPy co-modified CCALP LDHs were synthesized to improve the Cr(VI) removal efficiency. Both preparation and adsorption process parameters influenced the Cr(VI) removal efficiency. The Langmuir model fit well with the Cr(VI) adsorption data with the theoretical maximum adsorption capacity of 845.25 mg g^{-1}, contributing to the monolayer adsorption. The kinetic results showed that the Cr(VI) adsorption on CCALP was consistent with the AFO model, meaning the complexity and multiple kinetic stages of Cr(VI) adsorption. The characterization test of CCALP before and after Cr(VI) adsorption and DFT results confirmed that compared to the other prepared adsorbents, CCALP exhibited the maximum E_{ads} of Cr(VI) due to the electrostatic interaction, ion exchange, complexation and reduction mechanism. Therefore, CCALP has the application potential for treating Cr(VI)-contaminated wastewater.

Data availability

This study was carried out using publicly available data from [Science data bank] at [**https://www.scidb.cn/en/s/aqq67r**] with data DOI: **https://doi.org/10.57760/sciencedb.13100**.

Author contributions

Wenyan He: conceptualization, investigation, methodology, analysis, writing-review & editing, funding acquisition, validation; Kaijie Ye: software, data curation, analysis, visualization, editing; Mi Zhang: investigation, methodology, analysis, validation; Sheng Bai: methodology, analysis, data curation; Siyan Xu: visualization, methodology, data curation; Kuo Fang: software, analysis, review & editing.

Conflicts of interest

There are no conflicts to declare.

Acknowledgements

References

1 N. D. Nnaji, H. Onyeaka, T. Miri and C. Ugwa, Bioaccumulation for heavy metal removal: a review, *SN. Appl. Sci.*, 2023, **5**, 125, DOI: **10.1007/s42452-023-05351-6**.

2 Y. Xu, J. Chen, R. Chen, P. Yu, S. Guo and X. Wang, Adsorption and reduction of chromium (VI) from aqueous solution using polypyrrole/calcium rectorite composite adsorbent, *Water Res.*, 2019, **160**, 148–157, DOI: **10.1016/j.watres.2019.05.055**.

3 D. Bao, H. Wang, W. Liao and H. Q. Li, Multi-Metal Modified Layered Double Hydroxides for Cr(VI) and Fluoride Ion Adsorption in Single and Competitive Systems: Experimental and Mechanism Studies, *Environ. Eng. Sci.*, 2020, **37**, 623–636, DOI: **10.1089/ees.2020.0041**.

4 P. Liang, S. J. Liu, M. Li, W. Z. Xiong, X. Y. Yao, T. R. Xing and K. X. Tian, Effective adsorption and removal of Cr(VI) from wastewater using magnetic composites prepared by synergistic effect of polypyrrole and covalent organic frameworks, *Sep. Purif. Technol.*, 2024, **336**, 126222, DOI: **10.1016/j.seppur.2023.126222**.

5 C. H. Tseng, I. H. Lee and Y. C. Chen, Evaluation of hexavalent chromium concentration in water and its health risk with a system dynamics model, *Sci. Total Environ.*, 2019, **669**, 103–111, DOI: **10.1016/j.scitotenv.2019.03.103**.

6 V. E. Pakade, N. T. Tavengwa and L. M. Madikizela, Recent advances in hexavalent chromium removal from aqueous solutions by adsorptive methods, *RSC Adv.*, 2019, **9**, 26142–26164, DOI: **10.1039/C9RA05188K**.

7 F. B. Yao, M. C. Jia, Q. Yang, K. Luo, F. Chen, Y. Zhong, L. He, Z. J. Pi, K. J. Hou, D. B. Wang and X. M. Li, Electrochemical Cr(VI) removal from aqueous media using titanium as anode: Simultaneous indirect electrochemical reduction of Cr(VI) and in-situ precipitation of Cr(III), *Chemosphere*,

2020, **260**, 127537, DOI: **10.1016/j.chemosphere.2020.127537**.

8 S. Imdad, R. K. Dohare, M. Agarwal and A. Srivastava, Efficient removal of Cr(VI) from wastewater using recycled polymer-based supported ionic liquid membrane technology, *Sep. Purif. Technol.*, 2023, **327**, 124908, DOI: **10.1016/j.seppur.2023.124908**.

9 P. Thiripelu, J. Manjunathan, M. Revathi and P. Ramasamy, Removal of hexavalent chromium from electroplating wastewater by ion-exchange in presence of Ni(II) and Zn(II) ions, *J. Water Process Eng.*, 2024, **58**, 104815, DOI: **10.1016/j.jwpe.2024.104815**.

10 M. R. Wu, Y. N. Xu, C. X. Zhao, H. N. Huang, C. Liu, X. Duan, X. M. Zhang, G. H. Zhao and Y. G. Chen, Efficient nitrate and Cr(VI) removal by denitrifier: the mechanism of S. oneidensis MR-1 promoting electron production, transportation and consumption, *J. Hazard. Mater.*, 2024, **469**, 133675, DOI: **10.1016/j.jhazmat.2024.133675**.

11 K. Q. Lu, M. M. Gao, B. Sun, M. Wang, S. G. Wang and X. H. Wang, Simultaneous removal of Cr and organic matters via coupling Cr-Fenton-like reaction with Cr flocculation: The key role of Cr flocs on coupling effect, *Chemosphere*, 2022, **287**, 131991, DOI: **10.1016/j.chemosphere.2021.131991**.

12 A. Hasanzadeh, M. Alizadeh, N. Ajalli, J. Azamat and M. Jahanshahi, Molecular dynamic simulation and artificial neural network (ANN) modeling of the functionalized graphene oxide membranes on Cr (VI) ion removal through electrodialysis method, *J. Mol. Liq.*, 2023, **383**, 122083, DOI: **10.1016/j.molliq.2023.122083**.

13 X. Yang, B. Wang, P. Zhang, X. Song and F. Cheng, Adsorption and reduction of Cr(VI) by N, S co-doped porous carbon from sewage sludge and low-rank coal: Combining experiments and theoretical calculations, *Sci. Total Environ.*, 2024, **912**, 169265, DOI: **10.1016/j.scitotenv.2023.169265**.

14 Y. Y. Zhao, Z. Xu, X. Chen, M. Q. Deng, P. Li, W. Gao, J. Y. Li and X. M. Zhang, Enhancement of adsorption performance for I_2 and Cr(VI) by the metal-organic framework UiO-66-NH_2 via post-synthetic modification, *J. Environ. Chem. Eng.*, 2024, **12**, 111950, DOI: **10.1016/j.jece.2024.111950**.

15 R. Ishtiaq, N. Zahra, S. Iftikhar, F. Rubab, K. Sultan, A. Abbas, S. Lam, Z. H. Jaffari and K. Y. Park, Adsorption of Cr(VI) ions onto fluorine-free niobium carbide (MXene) and machine learning prediction with high precision, *J. Environ. Chem. Eng.*, 2024, **12**, 112238, DOI: **10.1016/j.jece.2024.112238**.

16 T. E. Khalil, A. H. Abdel-Salam, L. A. Mohamed, E. El-Meligy and A. El-Dissouky, Crosslinked modified chitosan biopolymer for enhanced removal of toxic Cr(VI) from aqueous solution, *Int. J. Biol. Macromol.*, 2023, **234**, 123719, DOI: **10.1016/j.ijbiomac.2023.123719**.

17 N. Bounab, L. Duclaux, L. Reinert, A. Oumedjbeur, F. Muller, I. Di Carlo and C. Boukhalfa, Ferrihydrite coating on kaolinite assisted by ultrasound for improving Cr(VI) adsorption in aqueous solutions, *Appl. Clay Sci.*, 2024, **250**, 107287, DOI: **10.1016/j.clay.2024.107287**.

18 S. X. Zhang, S. S. Yi, S. S. Yang and D. L. Chen, Novel montmorillonite/jute composites functionalized with polyethyleneimine and cetyltrimethylammonium bromide for Cr(VI) adsorption, *Appl. Clay Sci.*, 2024, **249**, 107235, DOI: **10.1016/j.clay.2023.107235**.

19 A. Auwalu, L. L. Tong, S. Ahmad, H. Y. Yang, Z. N. Jin and S. Yan, Preparation and application of metal ion-doped CoMgAl-hydrotalcite visible-light-driven photocatalyst, *Int. J. Ind. Chem.*, 2019, **10**, 121–131, DOI: **10.1007/s40090-019-0178-3**.

20 X. Tan, Y. J. Zhang, M. Liu, J. M. Cao, G. L. Duan, J. Cui and A. J. Lin, Ultrasonic-assisted preparation of interlaced layered hydrotalcite (U–Fe/Al-LDH) for high-efficiency removal of Cr(VI): Enhancing adsorption-coupled reduction capacity and stability, *Chemosphere*, 2022, **308**, 136472, DOI: **10.1016/j.chemosphere.2022.136472**.

21 G. C. Sun, J. Y. Zhang, X. Li, B. L. Hao, F. T. Xu and K. Q. Liu, Self-assembled morphology-controlled hierarchical Fe_3O_4 @LDH for Cr(VI) removal, *J. Environ. Chem. Eng.*, 2023, **11**, 110129, DOI: **10.1016/j.jece.2023.110129**.

22 M. Li, X. Chen, J. J. He, S. C. Liu, Y. Tang and X. G. Wen, Porous NiCo-LDH microspheres obtained by freeze-drying for efficient dye and Cr(VI) adsorption, *J. Alloys Compd.*, 2024, **976**, 173107, DOI: **10.1016/j.jallcom.2023.173107**.

23 K. H. Goh, T. T. Lim and Z. Dong, Application of layered double hydroxides for removal of oxyanions: a review, *Water Res.*, 2008, **42**, 1343–1368, DOI: **10.1016/j.watres.2007.10.043**.

24 X. Guan, X. Yuan, Y. Zhao, H. Wang, H. Wang, J. Bai and Y. Li, Application of functionalized layered double hydroxides for heavy metal removal: A review, *Sci. Total Environ.*, 2022, **838**, 155693, DOI: **10.1016/j.scitotenv.2022.155693**.

25 S. K. Qiu, D. Zhao, Y. Y. Feng, M. M. Li, X. F. Liang, L. S. Zhang, Y. Luo, K. Q. Zhang and F. Wang, Adsorption performance and mechanism of Ca-Al-LDHs prepared by oyster shell and pop can for phosphate from aqueous solutions, *J. Environ. Manage.*, 2022, **303**, 114235, DOI: **10.1016/j.jenvman.2021.114235**.

26 S. K. Qiu, M. M. Li, L. S. Zhang, M. Y. Yuan, M. H. Feng, C. B. Guo, K. Q. Zhang and F. Wang, Efficient degradation of disodium adenosine triphosphate by Ca-Al-LDH-supported Fe-activated persulfate and in situ adsorption of the phosphate products, *J. Cleaner Prod.*, 2023, **426**, 139106, DOI: **10.1016/j.jclepro.2023.139106**.

27 M. Kooravand, H. Haddadi, S. Asadpour, S. Farhadian, N. Sarmast and A. Asfaram, Simply synthesized Ca-Al-LDH-thiosulfate as adsorbent for removal of malachite green from aqueous solution, *Polyhedron*, 2023, **246**, 116653, DOI: **10.1016/j.poly.2023.116653**.

28 J. L. Milagres, C. R. Bellato, R. S. Vieira, S. O. Ferreira and C. Reis, Preparation and evaluation of the Ca-Al layered double hydroxide for removal of copper(II), nickel(II), zinc(II), chromium(VI) and phosphate from aqueous solutions, *J. Environ. Chem. Eng.*, 2017, **5**, 5469–5480, DOI: **10.1016/j.jece.2017.10.013**.

29 Z. Chen and K. Pan, Enhanced removal of Cr(VI) via in-situ synergistic reduction and fixation by polypyrrole/sugarcane bagasse composites, *Chemosphere*, 2021, **272**, 129606, DOI: **10.1016/j.chemosphere.2021.129606**.

30 Y. Yang, N. Chen, C. Feng, M. Li and Y. Gao, Chromium removal using a magnetic corncob biochar/polypyrrole composite by adsorption combined with reduction: Reaction pathway and contribution degree, *Colloids Surf., A*, 2018, **556**, 201–209, DOI: **10.1016/j.colsurfa.2018.08.035**.

31 L. Xiang, C. G. Niu, N. Tang, X. X. Lv, H. Guo, Z. W. Li, H. Y. Liu, L. S. Lin, Y. Y. Yang and C. Liang, Polypyrrole coated molybdenum disulfide composites as adsorbent for enhanced removal of Cr(VI) in aqueous solutions by adsorption combined with reduction, *Chem. Eng. J.*, 2021, **408**, 127281, DOI: **10.1016/j.cej.2020.127281**.

32 W. Fang, X. Jiang, H. Luo and J. Geng, Synthesis of graphene/SiO$_2$@polypyrrole nanocomposites and their application for Cr(VI) removal in aqueous solution, *Chemosphere*, 2018, **197**, 594–602, DOI: **10.1016/j.chemosphere.2017.12.163**.

33 H. Wang, X. Z. Yuan, Y. Wu, X. H. Chen, L. J. Leng, H. Wang, H. Li and G. M. Zeng, Facile synthesis of polypyrrole decorated reduced graphene oxide-Fe$_3$O$_4$ magnetic composites and its application for the Cr(VI) removal, *Chem. Eng. J.*, 2015, **262**, 597–606, DOI: **10.1016/j.cej.2014.10.020**.

34 D. Yang, Y. Chen, J. Li, Y. Li, W. Song, X. Li and L. Yan, Synthesis of calcium-aluminum-layered double hydroxide and a polypyrrole decorated product for efficient removal of high concentrations of aqueous hexavalent chromium, *J. Colloid Interface Sci.*, 2022, **607**, 1963–1972, DOI: **10.1016/j.jcis.2021.10.014**.

35 A. Idrisa, N. Hassana, R. Rashida and A. F. Ngomsik, Kinetic and regeneration studies of photocatalytic magnetic separable beads for chromium (VI) reduction under sunlight, *J. Hazard. Mater.*, 2011, **186**, 629–635, DOI: **10.1016/j.jhazmat.2010.11.101**.

36 Y. K. Mu, W. Y. He and H. Z. Ma, Enhanced adsorption of tetracycline by the modified tea-based biochar with the developed mesoporous and surface alkalinity, *Bioresour. Technol.*, 2021, **342**, 126001, DOI: **10.1016/j.biortech.2021.126001**.

37 N. Tang, C. G. Niu, X. T. Li, C. Liang, H. Guo, L. S. Lin, C. W. Zheng and G. M. Zeng, Efficient removal of Cd^{2+} and Pb^{2+} from aqueous solution with amino- and thiol-functionalized activated carbon: Isotherm and kinetics modeling, *Sci. Total Environ.*, 2018, **635**, 1331–1344, DOI: **10.1016/j.scitotenv.2018.04.236**.

38 X. Peng, Z. Yan, L. Hu, R. Zhang, S. Liu, A. Wang, X. Yu and L. Chen, Adsorption behavior of hexavalent chromium in aqueous solution by polyvinylimidazole modified cellulose, *Int. J. Biol. Macromol.*, 2020, **155**, 1184–1193, DOI: **10.1016/j.ijbiomac.2019.11.086**.

39 R. R. Shan, L. G. Yan, K. Yang, S. J. Yu, Y. F. Hao, H. Q. Yu and B. Du, Magnetic Fe$_3$O$_4$/MgAl-LDH composite for effective removal of three red dyes from aqueous solution, *Chem. Eng. J.*, 2014, **252**, 38–46, DOI: **10.1016/j.cej.2014.04.105**.

40 H. Zhang, X. Liu, Y. Chen, H. Kuang, H. Zhen, W. Zhang, H. Chen and Q. Ling, Construction of core-shell heterostructure containing sandwich-like nanoarray for high-performance supercapacitors, *J. Energy Storage*, 2023, **67**, 107647, DOI: **10.1016/j.est.2023.107647**.

41 L. Wang, M. Wang, H. Muhammad, Y. Sun, J. Guo and M. Laipan, Polypyrrole-Bentonite composite as a highly efficient and low cost anionic adsorbent for removing hexavalent molybdenum from wastewater, *J. Colloid Interface Sci.*, 2022, **615**, 797–806, DOI: **10.1016/j.jcis.2022.02.002**.

42 X. X. Wang, S. Q. Yu, Y. H. Wu, H. W. Pang, S. J. Yu, Z. S. Chen, J. Hou, A. Alsaedi, T. Hayat and S. H. Wang, The synergistic elimination of uranium (VI) species from aqueous solution using bi-functional nanocomposite of carbon sphere and layered double hydroxide, *Chem. Eng. J.*, 2018, **342**, 321–330, DOI: **10.1016/j.cej.2018.02.102**.

43 M. Qureshi, C. Viegas, S. O. D. Duarte, M. Girardi, A. Shehzad and P. Fonte, Camptothecin-loaded mesoporous silica nanoparticles functionalized with CpG oligodeoxynucleotide as a new approach for skin cancer treatment, *Int. J. Pharm.*, 2024, **660**, 124340, DOI: **10.1016/j.ijpharm.2024.124340**.

44 Z. Bashir, S. P. Church and D. Waldron, Interaction of water and hydrated crystallization in water-plasticized polyacrylonitrile films, *Polymer*, 1994, **35**, 967–976, DOI: **10.1016/0032-3861(94)90940-7**.

45 U. Riaz, N. Singh, A. Verma and E. S. Aazam, Studies on conducting polymer intercalated layered double hydroxide nanocomposites: Antituberculosis drug delivery agents, *Polym. Eng. Sci.*, 2020, **60**, 2628–2639, DOI: **10.1002/pen.25530**.

46 M. Dinari, F. Dadkhah, F. Azizollahi, G. Bateni and F. Bagherzadeh, Construction of new recoverable Ag-Fe$_3$O$_4$@Ca-Al LDH nanohybrids for visible light degradation of piroxicam, *Mater. Sci. Eng. B*, 2022, **278**, 115630, DOI: **10.1016/j.mseb.2022.115630**.

47 Y. Zhu, W. Shi, H. Gao, C. Li, W. Liang, Y. Nie, C. Shen and S. Ai, A novel aminated lignin/geopolymer supported with Fe nanoparticles for removing Cr(VI) and naphthalene: Intermediates promoting the reduction of Cr(VI), *Sci. Total Environ.*, 2023, **866**, 161379, DOI: **10.1016/j.scitotenv.2022.161379**.

48 L. Zhang, F. L. Fu and B. Tang, Adsorption and redox conversion behaviors of Cr(VI) on goethite/carbon microspheres and akaganeite/carbon microspheres composites, *Chem. Eng. J.*, 2019, **356**, 151–160, DOI: **10.1016/j.cej.2018.08.224**.

49 J. Wang, P. Wang, H. Wang, J. Dong, W. Chen, X. Wang, S. Wang, T. Hayat, A. Alsaedi and X. Wang, Preparation of Molybdenum Disulfide Coated Mg/Al Layered Double Hydroxide Composites for Efficient Removal of Chromium(VI), *ACS Sustain. Chem. Eng.*, 2017, **5**, 7165–7174, DOI: **10.1021/acssuschemeng.7b01347**.

50 J. Wang, Y. Liang, Q. Jin, J. Hou, B. Liu, X. Li, W. Chen, T. Hayat, A. Alsaedi and X. Wang, Simultaneous Removal of Graphene Oxide and Chromium(VI) on the Rare Earth

Doped Titanium Dioxide Coated Carbon Sphere Composites, *ACS Sustain. Chem. Eng.*, 2017, **5**, 5550–5561, DOI: **10.1021/acssuschemeng.7b00957**.

51 Y. Gao, C. Chen, X. Tan, H. Xu and K. Zhu, Polyaniline-modified 3D-flower-like molybdenum disulfide composite for efficient adsorption/photocatalytic reduction of Cr(VI), *J. Colloid Interface Sci.*, 2016, **476**, 62–70, DOI: **10.1016/j.jcis.2016.05.022**.

52 S. S. Baral, S. N. Das and P. Rath, Hexavalent chromium removal from aqueous solution by adsorption on treated sawdust, *Biochem. Eng. J.*, 2006, **31**, 216–222, DOI: **10.1016/j.bej.2006.08.003**.

53 A. E. Chávez-Guajardo, J. C. Medina-Llamas, L. Maqueira, C. A. S. Andrade, K. G. B. Alves and C. P. de Melo, Efficient removal of Cr(VI) and Cu(II) ions from aqueous media by use of polypyrrole/maghemite and polyaniline/maghemite magnetic nanocomposites, *Chem. Eng. J.*, 2015, **281**, 826–836, DOI: **10.1016/j.cej.2015.07.008**.

54 I. M. Lo, C. S. Lam and K. C. Lai, Hardness and carbonate effects on the reactivity of zero-valent iron for Cr(VI) removal, *Water Res.*, 2006, **40**, 595–605, DOI: **10.1016/j.watres.2005.11.033**.

55 M. Cotman, J. Zagorc-Končan and A. Žgajnar-Gotvajn, The relationship between composition and toxicity of tannery wastewater, *Water Sci. Technol.*, 2004, **49**, 39–46. **https://iwaponline.com/wst/article-pdf/49/31/39/421774/421739**.

56 M. Bhaumik, A. Maity, V. V. Srinivasu and M. S. Onyango, Enhanced removal of Cr(VI) from aqueous solution using polypyrrole/Fe$_3$O$_4$ magnetic nanocomposite, *J. Hazard.* *Mater.*, 2011, **190**, 381–390, DOI: **10.1016/j.jhazmat.2011.03.062**.

57 X. Song, W. L. Xiao, X. Chen, W. Q. Chen, H. Y. Mou and T. Q. Ao, Nanohybrid layered clay composite decorated with polyaniline for intensified Cr(VI) removal through enhanced Cr(VI) reduction, *Colloids Surf., A*, 2024, **697**, 134474, DOI: **10.1016/j.colsurfa.2024.134474**.

58 I. Said, M. R. Abukhadra, A. M. Rabie, A. A. Bakr, J. J. Shim and S. A. Ahmed, Facile Fabrication of ZnMgAl/LDH/Algae Composites as a Potential Adsorbent for Cr(VI) Ions from Water: Fabrication and Equilibrium Studies, *ACS Omega*, 2020, **48**, 31342–31351, DOI: **10.1021/acsomega.0c04842**.

59 J. Li, L. Yan, Y. Yang, X. Zhang, R. Zhu and H. Yu, Insight into the adsorption mechanisms of aqueous hexavalent chromium by EDTA intercalated layered double hydroxides: XRD, FTIR, XPS, and zeta potential studies, *New J. Chem.*, 2019, **43**, 15915–15923, DOI: **10.1039/c9nj03479j**.

60 C. Lei, X. Zhu, B. Zhu, C. Jiang, Y. Le and J. Yu, Superb adsorption capacity of hierarchical calcined Ni/Mg/Al layered double hydroxides for Congo red and Cr(VI) ions, *J. Hazard. Mater.*, 2017, **321**, 801–811, DOI: **10.1016/j.jhazmat.2016.09.070**.

61 Y. J. Ko, K. Choi, S. Lee, K. W. Jung, S. Hong, H. Mizuseki, J. W. Choi and W. S. Lee, Strong chromate-adsorbent based on pyrrolic nitrogen structure: An experimental and theoretical study on the adsorption mechanism, *Water Res.*, 2018, **145**, 287–296, DOI: **10.1016/j.watres.2018.08.033**.